Title: Metabolic Profiling of Dehydrodiisoeugenol Using Xenobiotic Metabolomics

Authors: Qian-Qian Lv, Xiao-Nan Yang, Dong-Mei Yan, Wei-Qing Liang, Hong-Ning Liu, Xiu-Wei Yang, Fei Li

PII: S0731-7085(17)31124-X
DOI: http://dx.doi.org/doi:10.1016/j.jpba.2017.07.045
Reference: PBA 11425

To appear in: *Journal of Pharmaceutical and Biomedical Analysis*

Received date: 3-5-2017
Revised date: 2-7-2017
Accepted date: 29-7-2017

Please cite this article as: Qian-Qian Lv, Xiao-Nan Yang, Dong-Mei Yan, Wei-Qing Liang, Hong-Ning Liu, Xiu-Wei Yang, Fei Li, Metabolic Profiling of Dehydrodiisoeugenol Using Xenobiotic Metabolomics, Journal of Pharmaceutical and Biomedical Analysishttp://dx.doi.org/10.1016/j.jpba.2017.07.045

Metabolic Profiling of Dehydrodiisoeugenol Using Xenobiotic Metabolomics

Qian-Qian Lv[a,b,1], Xiao-Nan Yang[a,1], Dong-Mei Yan[c], Wei-Qing Liang[d,*], Hong-Ning Liu[b], Xiu-Wei Yang[e], Fei Li[a,b,*]

[a]State Key Laboratory of Phytochemistry and Plant Resources in West China, Kunming Institute of Botany, Chinese Academy of Sciences, Kunming 650201, China

[b]Research Center for Differentiation and Development of Basic Theory of Traditional Chinese Medicine, Jiangxi University of Traditional Chinese Medicine, Nanchang 330004, China

[c]School of Pharmacy, Jiangxi University of Traditional Chinese Medicine, Nanchang 330004, China

[d]Center for Medicinal Resources Research, Zhejiang Academy of Traditional Chinese Medicine, Hangzhou 310007, China

[e]School of Pharmaceutical Sciences, Peking University Health Science Center, Peking University, Beijing 100191, China

[1]These authors contributed equally to this work

*Corresponding author:

Fei Li, Kunming Institute of Botany, Chinese Academy of Sciences, Kunming 650201, China. Tel: +86-871-65216953, Email: lifeib@mail.kib.ac.cn;

Wei-Qing Liang, Center for Medicinal Resources Research, Zhejiang Academy of Traditional Chinese Medicine, Hangzhou 310007, China. Tel: +86-571-88849079, Email: jxlwq22@163.com.

Highlights

- Metabolic map of dehydrodiisoeugenol from nutmeg was determined by metabolomics.

- Of the total 13 metabolites generated from dehydrodiisoeugenol, 7 are found to be novel.
- CYP1A1 plays the crucial role in the metabolism of dehydrodiisoeugenol.
- Two gut microbiota metabolites were elevated in mice urine after DDIE exposure

ABSTRACT

Dehydrodiisoeugenol (DDIE), a representative and major benzofuran-type neolignan in *Myristica fragrans* Houtt., shows anti-inflammatory and anti-bacterial actions. In order to better understand its pharmacological properties, xenobiotic metabolomics was used to determine the metabolic map of DDIE and its influence on endogenous metabolites. Total thirteen metabolites of DDIE were identified through *in vivo* and *in vitro* metabolism, and seven of them were reported for the first time in the present study. The identity of DDIE metabolites was achieved by comparison of the MS/MS fragmentation pattern with DDIE using ultra-performance chromatography electrospray ionization quadrupole time-of-flight mass spectrometry (UPLC-ESI-QTOFMS). Demethylation and ring-opening reaction were the major metabolic pathways for *in vivo* metabolism of DDIE. Recombinant cytochrome P450s (CYPs) screening revealed that CYP1A1 is a primary enzyme contributing to the formation of metabolites D1-D4. More importantly, the levels of two endogenous metabolites 2,8-dihydroxyquinoline and its glucuronide were significantly elevated in mouse urine after DDIE exposure, which explains in part its modulatory effects on gut microbiota. Taken together, these data contribute to the understanding of the disposition and pharmacological activities of DDIE *in vivo*.

Key words: Dehydrodiisoeugenol, Xenobiotic metabolomics, Metabolic profiling, UPLC-ESI-QTOFMS

1. Introduction

Lignans are a group of natural compounds derived from plants with a wide range of pharmacological activities, including anti-cancer, anti-microbial, anti-viral, anti-fungal and anti-atherosclerotic activities [1]. Various kinds of lignan compounds have been isolated and identified from the medicinal plant *Myristica fragrans* Houtt.. Benzofuran-type neolignans are the major components in *Myristica fragrans*. The contents of these neolignans can be used to evaluate the quality of the Traditional Chinese Medicine nutmeg (the seed of *M. fragrans*) [2]. Dehydrodiisoeugenol (2(3-methoxy-4-hydroxyphenyl)-3-methyl-5-(1-propenyl)-7-methoxy-2,3-dihydroben zofuran, DDIE), a benzofuran-type lignan, which has been recognized as a representative bioactive components of nutmeg. It was reported that DDIE exhibited various biological activities, including anti-lipid peroxidation [3], anti-bacterial action [4], and inhibition of hepatic drug metabolism enzyme [5]. DDIE shows the anti-inflammatory effect by inhibiting lipopolysaccharide-stimulated nuclear factor *κ*B activation and cyclooxygenase-2 expression in macrophages [6]. In addition, DDIE has been regarded as a model biphenyl and phenylcoumaran structural units and used as a skeleton to synthesize various of lignans [7]. Metabolism of DDIE has been investigated in rat, and several metabolites of DDIE were detected in rat urine and feces [8]. Despite its various biological activities and chemical characteristics have been studied, little is known about the metabolic behaviors of DDIE, especially in which cytochrome P450s (CYPs) are responsible for the generation of DDIE metabolites.

Recently, xenobiotic metabolomics plays an important role in determination of drug metabolites and its influence on endogenous metabolites through unbiased global analysis of low-molecular-weight molecules in biofluids [9, 10]. These results may determine the *in vivo* disposition of drug and its pharmacological properties after drug exposure [11]. Ultra-performance liquid chromatography electrospray ionization quadrupole time-of-flight mass spectrometry (UPLC-ESI-QTOFMS)-based metabolomics technologies have been widely applied to determine the metabolic

behaviors of drugs and xenobiotics, such as gefitinib [12], and noscapine [13]. The metabolic maps and the regulated endogenous metabolites could be used to explain the mechanism of action and toxicity of drugs/chemical substances. Therefore, the present study were performed by xenobiotic metabolomics based on UPLC-ESI-QTOFMS analysis, and aims to (i) clarify the metabolic pathways of DDIE in mice; (ii) evaluate the regulation of endogenous metabolites in mice after DDIE exposure; (iii) determine the drug-metabolizing enzymes involved in DDIE metabolism.

2. Materials and methods

2.1 Chemicals and reagents

Dehydrodiisoeugenol (DDIE) was obtained from Beta Biotechnology Co., Ltd (Nanchang, China). NADPH, chlorpropamide, and formic acid were purchased from Sigma-Aldrich (St. Louis, MO, USA). The liver microsomes including mouse liver microsomes (MLM) and human liver microsomes (HLM) for *in vitro* metabolism were purchased from Bioreclamationivt Inc. (Hicksville, NY, USA). Recombinant human CYP450 isoenzymes were provided by Xenotech, LLC (Kansas City, KS, USA). All other reagents were of the highest grade.

2.2 In vivo metabolism of DDIE

The *in vivo* metabolism of DDIE was conducted using male C57BL/6 mice (6 - 7 weeks age). The mice were provided by Slaccas Laboratory Animal Co., LTD. (Hunan, China). Mice were kept in cages for 1 week in a room at 23 ± 1 ℃with a light/dark cycle of 12/12 h and 50 - 60% related humidity with free access to tap water and standard rodent chow. All procedures were in accordance with study protocols approved by the Institutional Animal Care and Use Committee of the Kunming Institute of Botany, Chinese Academy of Sciences. The mice were randomly divided into two groups: control group and DDIE-treated group (n = 4 in each group). DDIE was suspended in a 0.5% (w/v) sodium carboxymethylcellulose (CMC-Na). For the DDIE-treated group, mice were administered with 200 mg/kg of DDIE by gavage,

and the mice were administrated with CMC-Na as control group. Urine and feces samples were collected for a period of 0-24 h using metabolic cages after treatment. All samples were stored at -80 °C until analysis.

Samples were prepared according to the method reported by Zhao, *et al* [14]. For urine samples preparation, 180 μL of 50% aqueous acetonitrile containing 5 μM of chlorpropamide (used as internal standard) was added into 20 μL of urine sample, and vortexed for 1 min. Then the samples were centrifuged at 18000 × *g* for 20 min at 4 ℃ to remove proteins and particulates. For feces samples preparation, 20 mg of each feces sample was homogenized with 10-fold of 50% aqueous acetonitrile, shaken for 20 min at room temperature. Then the samples were centrifuged at 18000 × *g* for 20 min at 4 ℃. After that, 100 μL of each supernatant was transferred to new Eppendorf tube, then 200 μL of 50% aqueous acetonitrile (containing 5 μM chlorpropamide) was added into each sample. The diluted samples were again centrifuged at 18000 × *g* for 20 min at 4 ℃. The supernatants were transferred to new tubes and 5 μL aliquot of each sample was injected for UPLC-ESI-QTOFMS analysis.

2.3 In vitro metabolism of DDIE

The *in vitro* metabolism of DDIE was performed in 96 wells plate. The 180 μL incubation system was consisted of 50 μM of DDIE, 0.5 g/mL of MLM or HLM in 20 mM phosphate buffer saline (PBS, pH 7.4). The system was pre-incubated at 37 ℃ for 5 min, then the reaction was started by adding 20 μL of 10 mM NADPH. The absence of NADPH but replaced by PBS in the incubation system was carried out as vehicle control. The reactions were incubated in a MicBio Ⅱ incubator at 37 ℃ and 800 rpm for 40 min. The liquids were transferred to new centrifuge tubes separately, and then 0.2 mL of cold acetonitrile was added in to each sample to stop the reaction. The samples were centrifuged at 18000 × *g* for 20 min at 4 ℃, 5 μL aliquot of the supernatant was injected for UPLC-ESI-QTOFMS analysis. The incubations were conducted in triplicates.

2.4 In vitro screening of CYPs involved in the metabolism of DDIE

The screening of CYP enzymes involved in the metabolism of DDIE was carried out in 96 wells plate. The incubation system including 50 μM DDIE as substrate, 2 pmol/ml of each recombined human P450 (control, CYP1A1, 1A2, 1B1, 2A6, 2B6, 2C19, 2C8, 2C9, 2D6, 2E1, 3A4, 3A5, and 4A11) in 20 mM PBS (pH = 7.4). The reaction was started by adding 20 μL of freshly prepared NADPH (10 mM). After 40 min incubation, the reaction was terminated by adding 200 μL of ice cold acetonitrile. Samples were centrifuged at 4 ℃, 18000 × *g* for 20 min, and 5 μL of each supernatant was injected for UPLC-ESI-QTOFMS analysis. Each reaction was conducted in triplicates.

2.5 UPLC-ESI-QTOFMS analysis

The urine, feces, and microsomal samples were analyzed by Agilent 1290 Series (Agilent, Santa Clara, CA, USA) UPLC system equipped with a 1290 Quat Pump. The compounds were separated by an XDB-C18 column (2.1 × 100mm, 1.8 μM, Agilent, Santa Clara, CA, USA), and the column temperature was maintained at 45 ℃. The flow rate was set at 0.3 mL/min. Solvent A was water contained 0.01% formic acid, and solvent B was composed of acetonitrile and 0.01% formic acid. The elution gradient was set as 2 to 98% B from 0 to 12 min, 98% B from 12 to 14 min and 2% B from 14 to 16 min. Both positive and negative ESI mode (6530 QTOFMS, Agilent, Santa Clara, CA, USA) were used for data collection. Nitrogen was used as collision gas and drying gas (9 L/min) which set at 350 °C. The nebulizer pressure was maintained at 35 psi, and the capillary voltage was set at 3.5 kV.

2.6 Data processing and Multivariate data analysis (MDA)

The software of MassHunter Workstation data Acquisition (Agilent, Santa Clara, CA, USA) was used for chromatographic and spectral data collection. Data alignment, generation of data matrix (consisted by peak areas, sample ID, unique *m/z* and retention time) were conducted by Mass Profiler Professional software (Agilent, Santa Clara, CA). The data matrix was then imported to SIMCA-P+13.0 software (Umetrics, Kinnelon, NJ, USA) followed by the previous description [15] for orthogonal

projection to latent structures-discriminant analysis (OPLS-DA). Potential DDIE metabolites and changed endogenous metabolites were initially identified by analyzing the ions contributing to the separation from control group in the *S*-loading plot of OPLS-DA.

2.7 Identification of xenobiotic and endogenous metabolites

The simultaneous identification of xenobiotic metabolites from DDIE and the changed endogenous metabolites were performed according the previous description [16]. After the potential DDIE metabolites was screened by *S*-plot, the tandem MS of selected metabolites was carried out in the targeted positive ESI mode by ramping collision energies from 9 to 13 eV. The chemical structures of DDIE metabolites were elucidated by interpreting their MS/MS fragmentation patterns. Seven Golden Rules [17] was used to calculate the mass error based on the elemental compositions of each metabolite. The structure of endogenous metabolites was preliminarily searched in METLIN and HMDB database and further identified by the MS/MS fragmentation patterns.

2.8 Data analysis

The values of experiments were presented as mean ± SEM. Statistical analysis was performed by using Prism v. 6 (GraphPad Software, San Diego, CA, USA). The values of $p < 0.05$ were considered significant.

3. Results and discussion

3.1 Metabolic profiling of DDIE in mice

Xenobiotic metabolomics is a powerful tool to determine the metabolites of xenobiotics [18], and may determine its potential pharmacological action through its regulation of endogenous metabolites [19]. Compare to other conventional models, Ultra-Performance Liquid Chromatography Electrospray Ionization Quadrupole Time-of-Flight Mass Spectrometry (UPLC-ESI-QTOFMS)-based metabolomics could quickly, accurately, and simultaneously identify xenobiotic metabolites and

endogenous metabolites altered by xenobiotics exposure. Previous studies reported that nine metabolites of DDIE were detected in rat liver microsome, urine and feces [8, 20]. In the present study, using xenobiotic metabolomics seven novel DDIE metabolites were identified, and the levels of two endogenous metabolites were changed in mouse urine by DDIE exposure which contributed to the understanding of its pharmacological effects.

The *in vivo* metabolism of DDIE was conducted in male C57BL/6 mice and the metabolite ions were analyzed by UPLC-ESI-QTOFMS in full scan ESI^+ mode because the signal response of DDIE in ESI^- mode is weak. The metabolites in urine and feces of DDIE-treated mice were well separated from vehicle mice in OPLS-DA model (Fig. S1A and C). The *in vivo* metabolites were further determined through the loading scatter *S*-plot (Fig. S1B and D). In urine sample, two phase I metabolites (**D7** and **D11)** and two phase II metabolites (**D9** and **D10**) were detected. The measurement of molecular ions weight and major fragment ion indicated that **D9** and **D10** were glucuronide adducts of parent DDIE and **D6**, respectively, and **D11** was a ring-opening (according to the previous report [8]) product generated from parent DDIE. In feces, four metabolites (**D6**, **D7**, **D12** and **D13**) were detected, but the tandem MS spectrum of **D13** was not obtained under the present condition. The high abundant parent DDIE was excreted through both urine and feces (Fig. 2A). The two glucuronidation metabolites **D9** and **D10** were excreted in urine only, in contrast, three phase I metabolites **D6**, **D12** and **D13** were excreted in feces only. The addition of glucuronic acid to DDIE and its metabolites will increase their hydrophilicity, leading to the quick excretion from the body. Combined the metabolites from the same type of metabolic pathway, we found that demethylation was the main reaction in DDIE metabolic process *in vivo* (Fig. 2B).

3.2 In vitro metabolism of DDIE in mouse liver microsome (MLM) and in human liver microsome (HLM)

The metabolic rate of drug frequently shows the species differences, especially in human and animal. To clarify the metabolic differences of DDIE between mice and

human, *in vitro* metabolisms of DDIE were conducted using mouse liver microsomal (MLM) and human liver microsomal (HLM) incubation models.

UPLC-ESI-QTOFMS coupled with OPLS-DA modeling was conducted to examine the difference between DDIE treatment and vehicle group in HLM. The DDIE treatment and control group in HLM could be well separated by the OPLS-DA model (Fig. 1A). The *in vitro* metabolites of DDIE have been further determined in the *S*-plot (Fig. 1B) according to their trending plots (example of **D3** and **D6** shown in Fig. 1C and D). Overall, total eight phase I metabolites (**D1 - D8**) of DDIE were identified in DDIE-treated HLM. Among these metabolites, **D7** was not found in MLM incubation system (Fig. 2C and Supplementary Table 1). The spectrographic peaks of **D1** and **D2** were closely similar, suggesting that **D1** and **D2** were the stereoisomer. Metabolites **D5**, **D7**, **D8** have been reported previously [8, 20]. Metabolites **D3**, **D4**, and **D6** were found in both MLM and HLM incubation systems and determined as novel metabolites. The percentage of whole metabolites of DDIE was shown in Figure 2C. The parent DDIE was the main component in both MLM and HLM incubation systems. The percentages of DDIE were 68.75% and 94.38% in MLM and HLM, respectively, suggesting that DDIE is more stable in HLM than MLM. As shown in Fig 2D, the demethylated metabolites (17.31%) and hydroxylated metabolites (13.95%) were the major products of DDIE in MLM incubation system. In HLM incubation system, the hydroxylation was the main metabolic pathway of DDIE metabolism (the percentage of hydroxylated metabolites of DDIE in HLM incubations was 4.80%). The metabolic rate of DDIE was 31.25% in MLM, which was higher than that in HLM (5.62%), suggesting that DDIE will be more stable in human than in mice. DDIE metabolism has been investigated in rat liver microsomes, and six metabolites were identified [8]. However, only part of these metabolites was detected in MLM, and seven novel metabolites were determined in MLM, suggesting metabolic differences of DDIE between rat and mice. These data demonstrated the metabolic differences for DDIE among human, rat and mice.

3.3 Structure identification of DDIE metabolites

The OPLS-DA analysis initially provided the potential metabolites of DDIE. Furthermore, tandem MS fragmentography was carried out to identify the chemical structures of these metabolites. Compared to the negative ion mode, DDIE showed stronger response to ESI positive ion mode that was selected to collect data. In the MS/MS fragmentation mode, the precursor ions $[M+H]^+$ and the retention time of the metabolites were locked to obtain daughter ions spectrum. The observed *m/z* of MS/MS fragment ions were shown in Supplementary Table 1, and the tandem MS spectrum and fragmentation patterns of new metabolites were presented in Fig. 3.

DDIE (**D0**) was calculated as $C_{20}H_{22}O_4$ based on the accurate mass measurement *m/z* 327.1597. The main MS/MS fragmentation ions of DDIE were 295, 203, 188, 171, 163 and 151. Metabolites **D1**, **D2**, **D3**, **D4** and **D5** were calculated as $C_{20}H_{22}O_5$ based on their excimer ions, and higher by 16 Da (O) than DDIE, showing that they were the hydroxylation products of DDIE. The elimination of the group of 18 (H_2O) and 57 (C_3H_5O) suggested the existence of 3-hydroxy-prop-1-enyl in metabolites **D1** and **D2**. The product ions at *m/z* 219 and 204 in **D1** and **D2** were higher by 16 Da than the product ions of DDIE at *m/z* 203 and 188, and *m/z* 163 and 151 in **D1** and **D2** were the similar product ions in DDIE, suggested that **D1** and **D2** were C9'-hydroxyl products of DDIE. The MS/MS fragments of **D1** were similar to those of **D2** (Fig. 3A)**,** indicating that **D1** and **D2** were one couple of stereoisomers. Compared to **D1**, **D2** showed higher abundance, which was consistent with M-6 of DDIE generated from rat liver microsome [8]. **D3** produced the daughter ions by eliminating the group of H_2O, C_2H_3 and C_3H_5O, indicating the C7'-hydroxylation and the rearrangement of C=C double bond of DDIE (Fig. 3B). The group of 41(C_3H_5) and 15(CH_3) were lost in **D4**, and the daughter ions at *m/z* 219, 188 and 179 of **D4** were higher by 16 Da than the daughter ions of DDIE at *m/z* 203, 171 and 163, suggesting that **D4** was C4'-hydroxyl or C6'-hydroxyl metabolite of DDIE (Fig. 3C). The product ions at *m/z* 203, 188 and 171 of **D5** were similar to the product ions found in DDIE and the *m/z* 167 was higher by 16 Da than the product ion of DDIE at *m/z* 151, indicating that **D5** was the hydroxylation metabolites on the left benzene ring, and the position C5-hydroxylation was identified by ^{1}H NMR in previous report [8].

Metabolites **D6** and **D7** were deduced as $C_{19}H_{20}O_4$ based on the accurate mass of *m/z* 313.1433 and *m/z* 313.1436, and both metabolites were lower by 14 Da (CH_2) than DDIE. In addition, the product ions at *m/z* 171 and 151 of **D6** were similar to the product ions found in DDIE and the *m/z* 189 was lower by 14 Da than the product ion of DDIE at *m/z* 203, indicating that **D6** was the C3'-demethylation metabolite of DDIE (Fig. 3D). The product ions at *m/z* 203, 188 and 163 of **D7** were similar to the product ions found in DDIE and the *m/z* 123 was lower by 14 Da than the product ion of DDIE at *m/z* 137, showing that **D7** was the C3-demethylation metabolite of DDIE. The elimination of the group of 29 (CHO) and 55(C_3H_3O) from metabolite **D8** suggested the existence of aldehyde group. It was calculated as $C_{20}H_{20}O_5$ based on the accurate mass of *m/z* 341.1380, and was 2 Da (H_2) lower than **D1**. The product ion at *m/z* 217 of **D8** was also 2 Da lower than product ion of **D1** at *m/z* 219, indicating **D8** was the C9'-hydroxylation and oxidation product of DDIE.

Metabolite **D9** was deduced as $C_{26}H_{30}O_{10}$ based on the accurate mass of *m/z* 503.1874, and was 176 Da ($C_6H_8O_6$) higher than DDIE. The product ions at *m/z* 327, 203 and 163 of **D9** were the same as the product ions found in DDIE, indicating that **D9** was glucuronic acid-conjugated product of DDIE (Fig. 3E). Metabolite **D10** was calculated as $C_{25}H_{28}O_{10}$ based on the accurate mass of *m/z* 489.1733, and was 176 Da ($C_6H_8O_6$) higher than **D6** or **D7**. The daughter ions at *m/z* 313 and 203 were similar to the product ions found in **D7**, suggesting that **D10** was glucuronic acid-conjugated product of **D7** (Fig. 3F).

The group of CH_3, CH_2O and C_3H_5 could be eliminated from **D12**, thus indicating that **D12** exists allyl group. It was calculated as $C_{19}H_{22}O_4$ based on the accurate mass of *m/z* 315.1580, and was 2 Da (H_2) higher than **D7**. The product ion at *m/z* 205 of **D12** was also 2 Da higher than product ion of **D7** at *m/z* 203, indicating **D12** was the ring-opening product of **D7** (Fig. 3G).

The tandem MS spectrum of **D11** and **D13** were not obtained under the present condition. The accurate mass at *m/z* 329.1727 of **D11** indicated **D11** was the ring-opening product of DDIE. The accurate mass at *m/z* 299.1643 of **D13** suggested that **D13** was a product of a series of complex reaction including demethylation,

ring-opening reaction, rearrangement and dihydroxylation. Both the two metabolites have been reported in the previous study [8].

3.4 Screening the CYPs involved in DDIE metabolism

To clarify the human phase I enzymes involved in DDIE metabolism, a panel of recombinant human P450s including CYP1A1, 1A2, 1B1, 2A6, 2B6, 2C19, 2C8, 2C9, 2D6, 2E1 3A4, 3A5 and 4A11 were incubated with DDIE individually. Table 1 demonstrated that the metabolism of DDIE was mediated by multiple P450s including CYP1A1, 1A2, 1B1, 2C19, 2C8, 2C9, 2D6, 3A4 and 3A5. CYP2A6, 2B6, 2E1 and 4A11 did not participate in the biotransformation of DDIE. As shown in the table 1, among all the examined P450s, CYP1A1 was an important enzyme which involved in DDIE metabolism as evidenced by the formation of nearly all DDIE metabolites except for **D6**. The metabolic rates of **D1**, **D2,** and **D4** by CYP1A1 were 96.82, 92.92, and 91.25%, respectively. In addition, the major product **D6** was metabolized by CYP2Cs including CYP2C19, 2C8 and 2C9, this result demonstrated that the CYP2Cs were primary enzymes to the DDIE metabolism. CYP3A4 was also an important enzyme because it was responsible for the production of **D1**-**D5** and **D7**, and the metabolic rate of **D5** was 58.24%. Metabolite **D3** was catalyzed by all of the active isoenzymes. Among these isoenzymes, CYP1A1 acted as the key role in formation of **D3**. Interestingly, two demethylation metabolites **D6** and **D7** were catalyzed by several different isoenzymes. CYP2C19, 2C8 and 2C9 were responsible for **D6** production, while the active enzymes for **D7** production were identified as CYP1A1, 1A2, 3A4 and 3A5. The most active enzyme for the formation of **D8** was CYP2C19.

In general, CYPs catalyze phase I metabolic reactions of drugs, leading to the polarity increasing of the substrate molecules. Thus, CYPs have been regarded as the rate-limiting enzymes for drugs elimination [21]. To determine the role of individual CYPs in DDIE metabolism, a panel of recombined human CYPs was separately incubated with DDIE. As shown Table 1, the CYP1A1 acted important role in DDIE metabolism. CYP1A1 is a metabolic enzyme which not only expressed in liver but

also in lung, thymus, kidney, heart, brain and other tissues, especially in the lung [22], and it is involved in phase I xenobiotic and drug metabolism. In the present study, various metabolites of DDIE were produced by CYP1A1 implied that multiple tissues may involve in DDIE metabolism. CYP3A4 also exhibited a key effect on DDIE metabolism. In addition, CYP2C19, 2C8 and 2C9 acted crucial roles in generation of **D6**, the most abundant metabolite of DDIE. Therefore, CYP1A1, CYP2Cs and CYP3A4 are important isoenzymes contributing to DDIE metabolism *in vivo*, and inhibition of these CYPs may result in side-effects when co-administration with other drugs.

3.5 Influence on endogenous metabolites in mouse urine by DDIE exposure

To determine the potential endogenous metabolites influenced by DDIE treatment, the mouse urine was analyzed by the approach of metabolomics. In the loading scatter *S*-plot of OPLS-DA, two endogenous metabolites (**I** and **II**) also contributed to the separation of DDIE treatment group from vehicle group (Fig. S1B). Both of the metabolites **I** and **II** in mouse urine significantly increased after exposure to DDIE (Fig. 4A and C). The chemical structure of these two altered metabolites were preliminarily determined by Seven Golden Rules [17] and by searching the METLIN and HMDB database. The chemical formula of metabolite **I** was calculated as $C_9H_8NO_2$ based on the molecular ion $[M+H]^+$ at *m/z* 162.0539 and **II** was calculated as $C_{15}H_{15}NO_8$ based on the molecular ion $[M+H]^+$ at *m/z* 338.0862. Furthermore, tandem MS spectrometry was carried out to confirm the chemical structure of the two metabolites. The fragment ions of metabolite **I** (144, 116, 89) were consisted with those of 2,8-dihydroxyquinoline [16], suggesting that **I** was 2,8-dihydroxyquinoline (Fig. 4B). Diagnostic loss of 176 Da ($C_6H_8O_6$) indicated metabolite **II** was a glucuronic acid-conjugated product, and the main fragment ions (162, 113) were consisted with those of 2,8-dihydroxyquinoline-glucuronide [23], suggested that II was 2,8-dihydroxyquinoline-glucuronide (Fig. 4D).

It reported that the dihydroxyquinoline could be transformed from quinolone by *Pseudomonas* species [24], and also could be produced by gut microbiota or

mammalian tissues [25]. Previous study demonstrated that the dihydroxyquinoline glucuronide could be detected only in conventional mouse serum, but could not be found in germ-free mice [26]. The production of both 2,8-dihydroxyquinolin and its glucuronide was significantly elevated in mouse urine by the antioxidant drug tempol [16], which can protect against high-fat diet induced obesity through regulating the composition of gut micriobiota [27]. One early study reported that DDIE could protect against *streptococcus mutans* [4]. One recent study found that nutmeg attenuated the levels of four uremic toxins generated by gut microbiota, leading to the decrease of intestinal tumorigenesis in *Apc*$^{min/+}$ mice [28]. These evidences suggest that DDIE might perform its pharmacological effects through its modulation of gut microbiota, including anti-inflammatory and anti-bacterial action.

4. Conclusion

In summary, xenobiotic metabolomics was found to be a useful tool for the identification of xenobiotic and endogenous metabolites during drug treatment or xenobiotic exposure. Drug metabolite profiling of DDIE-treated mice in this study indicated that total thirteen metabolites (seven are novel) were identified, and demethylation and ring-opening reaction were the major metabolic pathways for *in vivo* metabolism of DDIE. A comprehensive *in vivo* metabolic map of DDIE was generated through use of xenobiotic metabolomics (Fig. 5). A panel of CYPs screening revealed that CYP1A1 is a primary enzyme contributing to the formation of metabolites D1-D4. The change in endogenous metabolites indicated that DDIE performs its pharmacological activities via its modulatory effects on gut microbiota, which may be involved in the anti-bacterial and anti-inflammatory actions of this compound.

Acknowledgments

This work was supported by the Thousand Young Talents Program of China and State Key Laboratory of Phytochemistry and Plant Resources in West China (52Y67A9211Z1) and Postdoctoral targeted funding, Ministry of Human Resources and Social Security of Yunnan Province, China (39Y732921261).

Conflict of interest

The authors have declared no conflict of interest.

References

[1] W.D. MacRae, Towers, G. N., Biological activities of lignans, Phytochem. Rev. 23(6) (1984) 1207-1220.
[2] Y. Wang, and Yang, X. W. , Quantitative Determination of Neolignanoids in the Seeds of Myristica fragrans, Mod. Chinese Medicine. 2 (2008) 004.
[3] M. Hattori, Yang, X. W., Miyashiro, H., and Namba, T., Inhibitory effects of monomeric and dimeric phenylpropanoids from mace on lipid peroxidation in vivo and in vitro, Phytother. Res. 7(6) (1993) 395-401.
[4] M. Hattori, Hada, S., Watahiki, A., Ihara, H., Shu, Y. Z., Kakiuchi, N., ... and Namba, T., Studies on Dental Caries Prevention by Traditional Medicines. X.: Antibacterial Action of Phenolic Components from Mace against Streptococcus mutans, Chem. Pharm. Bull. 34(9) (1986) 3885-3893.
[5] K.H. Shin, Kim, O. N., and Woo, W. S., Isolation of hepatic drug metabolism inhibitors from the seeds ofMyristica fragrans, Arch. Pharm. res. 11(3) (1988) 240-243.
[6] Y. Murakami, M. Shoji, A. Hirata, S. Tanaka, I. Yokoe, S. Fujisawa, Dehydrodiisoeugenol, an isoeugenol dimer, inhibits lipopolysaccharide-stimulated nuclear factor kappa B activation and cyclooxygenase-2 expression in macrophages, Arch. Biochem. Biophy. 434(2) (2005) 326-32.
[7] G.E.S. Domburg, V. N.; Zheibe, G. A., Thermal analysis of some lignin model compounds, J. Therm. Anal. 2 (1970) 419-428.
[8] F. Li, X.W. Yang, Metabolism of the lignan dehydrodiisoeugenol in rats, Planta Med. 77(15) (2011) 1712-7.
[9] F.J. Gonzalez, Z.Z. Fang, X. Ma, Transgenic mice and metabolomics for study of hepatic xenobiotic metabolism and toxicity, Expert opin. Drug Met. 11(6) (2015) 869-81.
[10] C.H. Johnson, A.D. Patterson, J.R. Idle, F.J. Gonzalez, Xenobiotic metabolomics: major impact on the metabolome, Annu. Rev. Pharmacol. 52 (2012) 37-56.
[11] B. Daviss, Growing pains for metabolomics: the newest'omic science is producing results--and more data than researchers know what to do with, The Scientist. 19(8) (2005) 25-29.
[12] X. Liu, Lu, Y., Guan, X., Dong, B., Chavan, H., Wang, J., ... and Li, F., Metabolomics reveals the formation of aldehydes and iminium in gefitinib metabolism, Biochem. Pharmacol. 97(1) (2015)

111-121.
[13] Z.Z. Fang, K.W. Krausz, F. Li, J. Cheng, N. Tanaka, F.J. Gonzalez, Metabolic map and bioactivation of the anti-tumour drug noscapine, Brit. J. Pharmacol. 167(6) (2012) 1271-86.
[14] Q. Zhao, Li, X M., Liu, H N., Gonzalez, F J., Li, F., Metabolic map of osthole and its effect on lipids, Xenobiotica (just-accepted). (2017) 1-38.
[15] A.D. Patterson, H. Li, G.S. Eichler, K.W. Krausz, J.N. Weinstein, A.J. Fornace, Jr., F.J. Gonzalez, J.R. Idle, UPLC-ESI-TOFMS-based metabolomics and gene expression dynamics inspector self-organizing metabolomic maps as tools for understanding the cellular response to ionizing radiation, Anal. Chem. 80(3) (2008) 665-74.
[16] F. Li, X. Pang, K.W. Krausz, C. Jiang, C. Chen, J.A. Cook, M.C. Krishna, J.B. Mitchell, F.J. Gonzalez, A.D. Patterson, Stable isotope- and mass spectrometry-based metabolomics as tools in drug metabolism: a study expanding tempol pharmacology, J. Proteom. Res. 12(3) (2013) 1369-76.
[17] T. Kind, O. Fiehn, Seven Golden Rules for heuristic filtering of molecular formulas obtained by accurate mass spectrometry, BMC Bioinformatics. 8 (2007) 105.
[18] C.G. Chen, F. J., LC-MS-based metabolomics in drug metabolism, Drug Metab. Rev. 39(2-3) (2007) 581-597.
[19] A. Fages, T. Duarte-Salles, M. Stepien, P. Ferrari, V. Fedirko, C. Pontoizeau, A. Trichopoulou, K. Aleksandrova, A. Tjonneland, A. Olsen, F. Clavel-Chapelon, M.C. Boutron-Ruault, G. Severi, R. Kaaks, T. Kuhn, A. Floegel, H. Boeing, P. Lagiou, C. Bamia, D. Trichopoulos, D. Palli, V. Pala, S. Panico, R. Tumino, P. Vineis, H.B. Bueno-de-Mesquita, P.H. Peeters, E. Weiderpass, A. Agudo, E. Molina-Montes, J.M. Huerta, E. Ardanaz, M. Dorronsoro, K. Sjoberg, B. Ohlsson, K.T. Khaw, N. Wareham, R.C. Travis, J.A. Schmidt, A. Cross, M. Gunter, E. Riboli, A. Scalbert, I. Romieu, B. Elena-Herrmann, M. Jenab, Metabolomic profiles of hepatocellular carcinoma in a European prospective cohort, BMC Med. 13 (2015) 242.
[20] F. Li, X.W. Yang, Analysis of anti-inflammatory dehydrodiisoeugenol and metabolites excreted in rat feces and urine using HPLC-UV, Biomedical chromatography: BMC. 26(6) (2012) 703-7.
[21] H. Iwata, Y. Tezuka, S. Kadota, A. Hiratsuka, T. Watabe, Identification and characterization of potent CYP3A4 inhibitors in Schisandra fruit extract, Drug Metab. Dispos. 32(12) (2004) 1351-8.
[22] D. Choudhary, I. Jansson, I. Stoilov, M. Sarfarazi, J.B. Schenkman, Expression patterns of mouse and human CYP orthologs (families 1-4) during development and in different adult tissues, Arch. Biochem. Biophy. 436(1) (2005) 50-61.
[23] Y. Zhen, K.W. Krausz, C. Chen, J.R. Idle, F.J. Gonzalez, Metabolomic and genetic analysis of biomarkers for peroxisome proliferator-activated receptor alpha expression and activation, Mol. Endocrinol. 21(9) (2007) 2136-51.
[24] O.P. Shukla, Microbial Transformation of Quinoline by a Pseudomonas sp., Am. Soc. Microbiol. 51(6) (1986) 1332-1342.
[25] P.Y. Hou, K.S. Bi, L.L. Geng, X. Zhao, X. Meng, B.J. Ma, Y. Zeng, X.F. Wang, X.H. Chen, Toxic effects of Euphorbia pekinensis Rupr. and development of a validated UPLC/MS/MS method for profiling of urine metabolic changes, Anal. Methods-UK 5(4) (2013) 953.
[26] W.R. Wikoff, A.T. Anfora, J. Liu, P.G. Schultz, S.A. Lesley, E.C. Peters, G. Siuzdak, Metabolomics analysis reveals large effects of gut microflora on mammalian blood metabolites, P. Natl. Acad. Sci. USA. 106(10) (2009) 3698-703.
[27] F. Li, C. Jiang, K.W. Krausz, Y. Li, I. Albert, H. Hao, K.M. Fabre, J.B. Mitchell, A.D. Patterson, F.J. Gonzalez, Microbiome remodelling leads to inhibition of intestinal farnesoid X receptor signalling

and decreased obesity, Nat. Commun. 4 (2013) 2384.
[28] F. Li, X.W. Yang, K.W. Krausz, R.G. Nichols, W. Xu, A.D. Patterson, F.J. Gonzalez, Modulation of colon cancer by nutmeg, J. Proteom. Res. 14(4) (2015) 1937-46.

Figure legends

Fig. 1. Metabolomics analysis of DDIE metabolites in human liver microsomal (HLM) incubation system. (A) Scores plot of an OPLS-DA model from HLM incubation mixture between control and DDIE-treated HLM. (B) *S*-loading plot of OPLS-DA model and partial enlarged detail of *S*-loading plot. (C) Trending plot of **D3** in control and DDIE-treated HLM. D, Trending plot of **D6** in HLM with and without DDIE. (●, control; ■, DDIE-treated HLM).

Fig. 2. *In vivo* and *in vitro* metabolism of DDIE. (A) Contents of DDIE metabolites in mouse urine and feces. (B) Comparison of the major metabolic pathway *in vivo*. (C) Metabolites of DDIE in mouse liver microsomal (MLM) and human liver microsomal (HLM) incubation systems. (D) Comparison of the major metabolic pathway *in vitro*. Reaction types: 1, hydroxylation; 2, demethylation; 3, oxidation; 4, ring-opening reaction. Data were presented as mean ± SEM. **D0** represents parent DDIE. N.D., not detected. *In vivo* analysis, the relative abundance was conducted based on the peak areas of ion counts and normalized by the peak area of internal standard. *In vitro* analysis, the sum of peak areas of total detected ion counts was integrated as 100%.

Fig. 3. Tandem MS spectrum and fragmentation pattern of novel DDIE metabolites. (A) Tandem MS spectrum and fragmentation pattern of **D1**. (B) Tandem MS spectrum and fragmentation pattern of **D3**. (C) Tandem MS spectrum and fragmentation pattern of **D4**. (D) Tandem MS spectrum and fragmentation pattern of **D6**. (E) Tandem MS spectrum and fragmentation pattern of **D9**. (F) Tandem MS spectrum and fragmentation pattern of **D10**. (G) Tandem MS spectrum and fragmentation pattern of **D12**. MS/MS fragmentation was conducted with collision

energy at 9 – 13 eV.

Fig. 4. Change of endogenous metabolites in mouse urine after exposure to DDIE. (A) Comparison of 2,8-dihydroxyquinoline between control groups and DDIE-treated group. (B) Tandem MS spectra and fragmentation pattern of 2,8-dihydroxyquinoline. (C) Comparison of 2,8-dihydroxyquinoline-*β*-D-glucuronide between control groups and DDIE-treated group. (D) Tandem MS spectra and fragmentation pattern of 2,8-dihydroxyquinoline-*β*-D-glucuronide. *, $p < 0.05$; **, $p < 0.01$.

Fig. 5. Metabolic map of DDIE. Structures of these metabolites were determined based on the exact mass measurement (mass error less than 10 ppm) and MS/MS fragments, and compared with the known metabolites reported by previous study. Reaction types: 1, hydroxylation; 2, demethylation; 3, oxidation; 4, ring-opening reaction; 5, rearrangement; 6, dehydroxylation; 7, glucuronidation. *novel metabolites identified in the present study.

Figure 1.

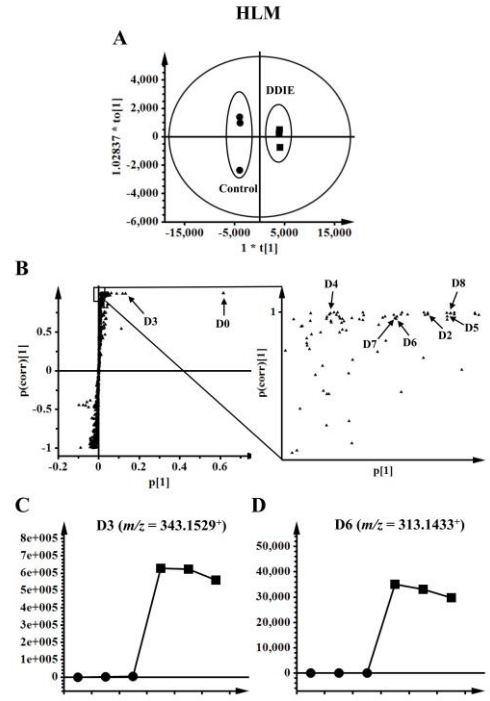

Figure 2.

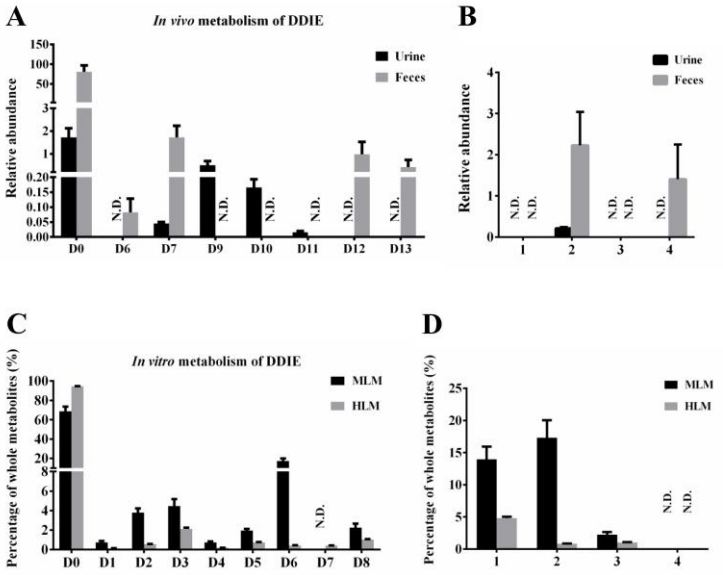

Figure 3.

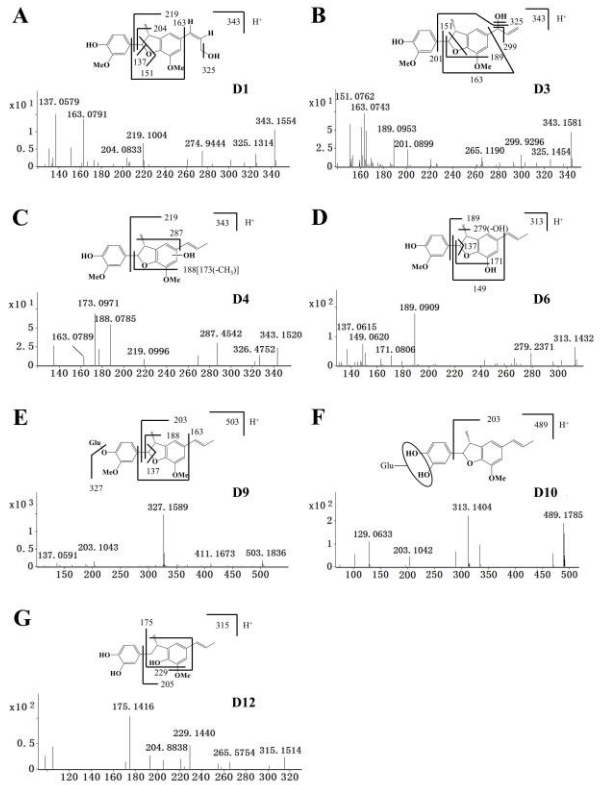

Figure 4.

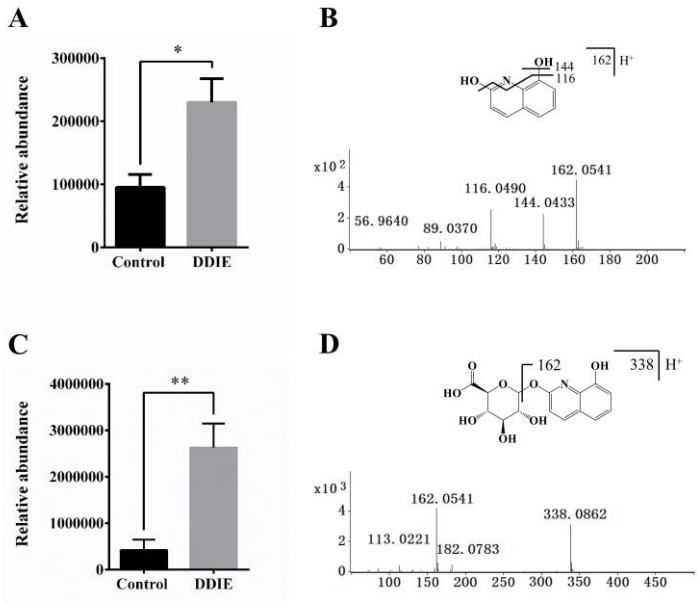

Figure 5.

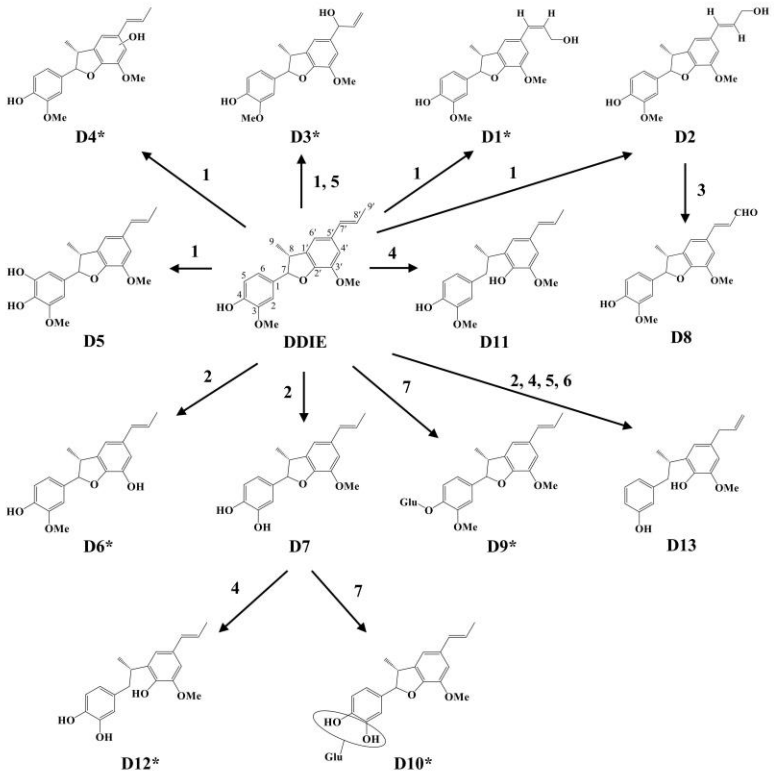

Table 1. Roles of CYP450s in the formation of DDIE metabolites.

No.	Enzyme	D1	D2	D3	D4	D5	D6	D7	D8
0	**Control**	–	–	–	–		–	–	–

1	**CYP1A1**	96.82	92.92	22.27	91.25	11.58	–	27.16	17.73
2	**CYP1A2**	–	1.05	8.09	–	8.23	–	17.05	9.84
3	**CYP1B1**	–	0.43	1.05	–	–	–	–	–
4	**CYP2A6**	–	–	–	–	–	–	–	–
5	**CYP2B6**	–	–	–	–	–	–	–	–
6	**CYP2C19**	–	–	48.83	–	–	45.64	–	65.53
7	**CYP2C8**	–	0.57	5.29	–	–	21.15	–	–
8	**CYP2C9**	–	–	0.75	–	–	33.22	–	–
9	**CYP2D6**	–	–	10.11	–	–	–	–	6.90
10	**CYP2E1**	–	–	–	–	–	–	–	–
11	**CYP3A4**	3.18	3.83	1.84	8.75	58.24	–	39.17	–
12	**CYP3A5**	–	1.20	1.78	–	21.95	–	16.63	–
13	**CYP4A11**	–	–	–	–	–	–	–	–

cDNA-expressed CYPs (control, CYP1A1, 1A2, 1B1, 2A6, 2B6, 2C19, 2C8, 2C9, 2D6, 2E1, 3A4, 3A5, and 4A11) were used to examine the roles of in individual CYPs in DDIE metabolism. All samples were analyzed by UPLC-ESI-QTOFMS. The total peak areas of each metabolite of DDIE from all the CYPs were set as 100%. All data are expressed as mean (n = 3).